Eur Biophys J (2008) 38:1–12
DOI 10.1007/s00249-008-0347-3

ORIGINAL PAPER

Energetics of subdomain movements and fluorescence probe solvation environment change in ATP-bound myosin

Michael J. Harris · Hyung-June Woo

Received: 25 January 2008 / Revised: 16 May 2008 / Accepted: 22 May 2008 / Published online: 21 June 2008

Abstract Energetics of conformational changes experienced by an ATP-bound myosin head detached from actin was studied by all-atom explicit water umbrella sampling simulations. The statistics of coupling between large scale domain movements and smaller scale structural features were examined, including the closing of the ATP binding pocket, and a number of key hydrogen bond formations shown to play roles in structural and biochemical studies. The statistics for the ATP binding pocket open/close transition show an evolution of the relative stability from the open state in the early stages of the recovery stroke to the stable closed state after the stroke. The change in solvation environment of the fluorescence probe Trp507 (scallop numbering; 501 in *Dictyostelium discoideum*) indicates that the probe faithfully reflects the closing of the binding pocket as previously shown in experimental studies, while being directly coupled to roughly the early half of the overall large scale conformational change of the converter domain rotation. The free energy change of this solvation environment change, in particular, is −1.3 kcal/mol, in close agreement with experimental estimates. In addition, our results provide direct molecular level data allowing for interpretations of the fluorescence experiments of myosin conformational change in terms of the de-solvation of Trp side chain.

Keywords Myosin · Muscle contraction · Molecular dynamics · Free energy · Fluorescence probe

M. J. Harris · H.-J. Woo (✉)
Department of Chemistry, University of Nevada,
Reno, NV 89557, USA
e-mail: woo@unr.edu

Introduction

Myosin-actin complexes constitute one of the best-characterized classes of motor proteins, which convert chemical free energy into mechanical work via ATP hydrolysis, driving muscle contractions (Vale and Milligan 2000; Spudich 2001). Significant strides in studies of the molecular mechanism of actomyosin action have been made possible, in particular, by recent determinations of high-resolution structures of myosin head in various conformational states (Rayment et al. 1993; Gulick et al. 1997; Dominguez et al. 1998; Geeves and Holmes 1999; Houdusse et al. 1999, 2000; Bauer et al. 2000; Houdusse and Sweeney 2001; Himmel et al. 2002; Gourinath et al. 2003). Together with the advances in single molecule studies of the dynamics in such motor complexes (Simmons et al. 1996; Ishijima et al. 1996; Baker et al. 1998), detailed dynamical descriptions of the classic swinging lever arm mechanism (Lymn and Taylor 1971; Spudich 2001) in molecular detail are being realized.

The conformational changes a myosin head is expected to undergo can roughly be divided into two classes: those while bound to actin and those while detached (or weakly bound). The power stroke occurs when the actin-bound myosin releases the bound phosphate (Pi) and changes its conformation from the pre-power stroke to rigor states, and is the major step producing work via the resulting rotation of the converter domain (from the 'up' to 'down' orientation) tightly connected to its lever arm. This restoration of the converter 'down' state is activated by actin with high efficiency, without which the corresponding reverse recovery stroke becomes the rate-limiting step of the basal ATPase activity of myosin (Gyimesi et al. 2008). The post-stroke myosin binds ATP, detaches from actin, and reprimes its lever arm from the rigor to pre-stroke orientations.

This reverse power stroke of the detached myosin with bound ATP, or the recovery stroke, is expected to be closely coupled to the closing of the ATP binding pocket that turns on the catalytic activity of the enzyme. The end-state of the recovery stroke catalyzes the hydrolysis of ATP, producing the pre-power stroke complex ready to re-bind to actin.

The energetics of substeps and stabilities of intermediates involved in the overall muscle contraction cycle constitute important details of the mechanism of motor action, for which biochemical kinetic studies have provided crucial guidance (Geeves and Holmes 1999). Although structurally one would expect the power stroke and recovery stroke to be roughly the reverse process of each other, their respective energetics are thought to differ considerably. The power stroke is the major step generating work via the sliding movement of actin filaments, and it is reasonable to expect the motor to have evolved to maximize the fraction of free energy expended during the conformational change while bound to actin (Geeves and Holmes 1999; Yu et al. 2007a). The recovery stroke, in contrast, occurs while detached, with the associated free energy change dissipated as heat.

Such an expectation is borne out by kinetic evidences which indicate that the energetics of the (pre-hydrolysis) open/close transition of an ATP-bound myosin is freely reversible (Málnási-Csizmadia et al. 2001a; b). The hydrolysis of ATP, activated by the closing of binding pocket in the post-recovery stroke conformation, presumably biases the isoenergetic conformational equilibrium by facilitating actin binding (Málnási-Csizmadia et al. 2001b; Kovács et al. 2002; Conibear et al. 2004; Málnási-Csizmadia et al. 2007; Gyimesi et al. 2008).

More direct and quantitative connections of the expected energetics to known structural information, including the roles played by key residues and local structural changes, can be achieved by methods of simulation studies based on high-resolution structures. Numerous computational studies have recently been performed to examine local energetic properties of myosin in a given conformational state, including normal mode and principal component analysis studies (Li and Cui 2004a; Zheng and Brooks 2005a, b; Mesentean et al. 2007), a molecular dynamics (MD) study of Pi-release (Lawson et al. 2004), a mixed quantum/classical dynamics study of ATP hydrolysis (Li and Cui 2004b), structure refinements of actin-bound myosin head using MD (Liu et al. 2006), local equilibrium simulations of two end-point conformations (Koppole et al. 2006), a modeling of mesoscale dynamics (Burghardt et al. 2007), and a coarse-grained simulation study (Takagi and Kikuchi 2007). Most recently, Yu et al. (2007a) have performed a free energy analysis of the open and closed states of the binding pocket within the two separate end-states of the recovery stroke, providing evidences for the coupling of the relative stability shift to the global conformational change. Also notable as a simulation study of the motor parts outside the myosin head is the work by Ganoth et al. (2006; 2007) on the related processive motor myosin V, where it was proposed that the ionic strength dependence of peptide conformational changes within the lever arm plays roles in the motor action.

A number of recent studies have considered large scale conformational changes of myosin head and its coupling to local structural events using computational means. With well-characterized structures of the myosin head without actin corresponding to the start and end-points of the conformational change, the recovery stroke is an ideal process amenable to computational approaches. A series of minimum energy studies have been reported (Fischer et al. 2005; Koppole et al. 2007), where a minimum energy pathway connecting the two end-points of the conformational change is sought computationally. The method leads to scenarios involving residues and their movements proposed to participate in the conformational change in sequence in a deterministic fashion, which neglect entropic contributions to the energetics of the global conformational equilibria. Experimental kinetic studies using fluorescence probes have estimated the enthalpic and entropic contributions to the free energy of open/close transition to be both large in magnitude and opposite in sign, which yield an overall free energy change that is close to zero [$\Delta H = T\Delta S \approx 14$ kcal/mol for ATP analog-bound myosin in Málnási-Csizmadia et al. (2001b)]. The steered (or targeted) MD offers a different option of exploring the relevant conformational spaces between the two reference states (Woo 2007; Yu et al. 2007b), although its implications are limited by the highly nonequilibrium nature of its dynamics.

At the expense of larger computational demands, full samplings of the conformational space using umbrella sampling can yield detailed information on the energetics of global as well as local structural events taking into account entropic effects. In umbrella samplings, a series of MD simulations are performed under constraints designed to bias and enhance sampling of conformational states within the space of a chosen set of low-dimensional reaction coordinates. Each simulation trajectory, when run sufficiently long, reaches equilibrium under its respective constraining potential, and the resulting set of trajectories can be analyzed and recombined to yield free energy data for the chosen set of structural changes of interest by subtracting off the effects of biases.

The appropriateness of the use of low-dimensional reaction coordinates for large scale conformational changes depends critically on the nature of the system under study. One of the topics where theoretical and computational

approaches have been applied heavily is the study of protein folding, which inevitably requires descriptions involving high-dimensional, rugged landscapes of conformational spaces. In an analogy to mechanical devices, the study of folding can be compared with the descriptions of the design or assembly of an engine. Conformational changes of motor proteins, in contrast, where the end-points of the change are well-defined and differ only by rigid body type rearrangements of subdomains that remain tightly folded, are analogous to highly optimized simple operations of a functional engine, which can be described using low-dimensional variables such as the position of piston or rotation angle of the wheel. It is thus misleading to presume that low-dimensional reaction coordinates could not adequately describe motor protein conformational changes. The suitability of a chosen set of coordinates, instead, should be judged explicitly by verifying the correlations of the progression of reaction coordinate values with known structural changes of the system. The simplicity of the free energy landscapes of motor protein conformational changes also implies that the time scale gap between the ns regime accessible with MD and the μs $\sim$ ms regime in conformational changes can be bridged by biased sampling, analogous to the case of a one-dimensional double-well potential with a high barrier, which can be sampled efficiently if the biasing potential effectively flattens the barrier.

In this paper, we report results of an extensive set of computational sampling of conformational states connecting the start and end-points of the recovery stroke, using umbrella samplings with constraints acting on a ΔRMSD reaction coordinate (Banavali and Roux 2005a, b; Faraldo-Gómez and Roux 2007; Arora and Brooks 2007) defined with respect to the near-rigor (R) and pre-stroke (P) crystal structures of scallop myosin (Himmel et al. 2002; Gourinath et al. 2003). An exploratory testing of a version of the basic computational methodology was reported earlier (Woo 2007), where a limited sampling of conformational spaces resulted in a free energy profile predominantly downhill for the repriming direction of the recovery stroke. The current paper is the report of a full-scale sampling with biological interpretations of results. The resulting collection of statistics provided sufficient data to analyze the convergence properties of the sampling. In particular, major novel features in the current work consist of the analysis of trajectories revealing the coupling of larger and smaller scale structural signatures of the conformational change in quantitative fashion in terms of free energy landscapes, and the validation of the computational results via comparisons with experiments on the Trp fluorescence probe. Such a direct cross validation of the energetics of detailed molecular level changes with experimental data has not been achieved in other computational studies so far.

Table 1 Comparison of residue numbers for scallop and *Dictyostelium discoideum* myosins

Scallop	Arg242	Gly463	Glu465	Asn481	Gln497	Trp507
Dictyostelium	Arg238	Gly457	Glu459	Asn475	Gln491	Trp501

Scallop myosin structures (Houdusse et al. 1999, 2000; Himmel et al. 2002; Gourinath et al. 2003), compared to *Dictyostelium discoideum* (Fisher et al. 1995; Smith and Rayment 1996; Bauer et al. 2000) used in other computational studies, offer the advantage of having the two main R and P reference crystallographic states for the full myosin head that include the intact converter domain/lever arm (Table 1). The relay loop, which contains the Trp fluorescence probe, is also well-resolved in both the R and P-state crystal structures of scallop myosin, while it is disordered in many *Dictyostelium* R-state structures (Fisher et al. 1995; Bauer et al. 2000). In addition, for scallop myosin, a third, "internally uncoupled" conformational state has also been identified (Himmel et al. 2002), where the SH1 helix is unwound and the converter domain is believed to be uncoupled from the lever arm.

Methods

System preparation and simulation conditions

The scallop myosin reference conformations were taken as the crystal structures from Himmel et al. (2002) (PDB ID 1KK7; R-state) and Gourinath et al. (2003) (PDB ID 1QVI; P-state). Procedures for building the model complexes have been described previously (Woo 2007). The myosin head simulated was truncated near the beginning of the lever arm (beyond Ala787; Fig. 1a, b). All simulations and analysis were done using CHARMM (Brooks et al. 1983) with version-27 force fields (MacKerell et al. 1998). The simulation boxes for each window had approximate dimensions of $150 \times 120 \times 70$ Å^3, containing roughly 35,500 water molecules [TIP3P model (Jorgensen et al. 1983)]. The SHAKE algorithm (van Gunsteren and Berendsen 1977) was used with a time step of 2 fs, and particle mesh Ewald (Darden et al. 1993) was used for electrostatics with periodic boundary conditions. The van der Waals cut off used was 10 Å. Simulations were run at constant temperature of 300 K, mostly with constant volume with occasional constant pressure simulations at 1 atm used to re-equilibrate the box as necessary. To prevent the protein from drifting out of the water box, its center of mass was constrained to the center of the box by a harmonic constraint with a force constant 10 kcal/mol Å^2.

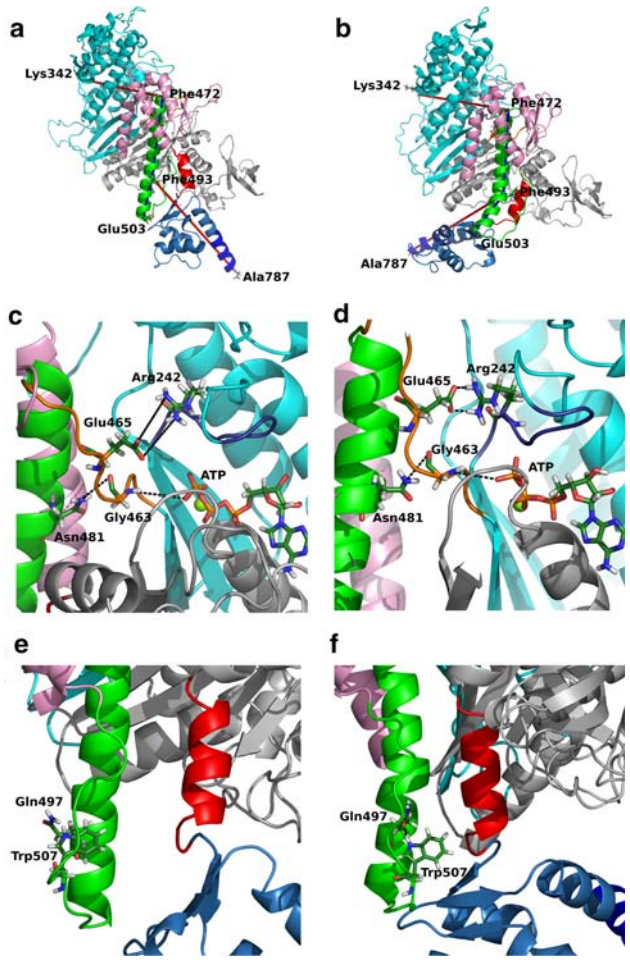

Fig. 1 Two different conformations representing the end-points of the recovery stroke, the near-rigor (R; *left column*) and pre-stroke (P; *right column*) states. Representative snapshots were taken from the umbrella sampling sets to produce the figures. **a**, **b** Converter domain rotation and relay helix kink formation, showing the residues used to define the angles (see "Methods"). **c**, **d** ATP binding pocket of the protein, showing the closing of the pocket signified by the hydrogen bond and salt bridge formations. **e**, **f** The change of environment of the fluorescence probe Trp507. The SH1 helix connected to the converter domain approaches the probe in the P-state, significantly reducing its solvent accessibility. The colors used for subdomains are as follows: upper 50 K (*cyan*), lower 50 K (*pink*), N-terminal (*gray*), relay helix (*green*), switch-2 (*orange*), P-loop (*dark blue*), SH1 helix (*red*), converter domain (*light blue*), lever arm (*blue*)

Umbrella sampling

In total, 34 windows were run in the umbrella sampling under constraints given by $u_n = k(\Delta y - \bar{y}_n)^2$, where k is the force constant, $\Delta y = y_R - y_P$ is the ΔRMSD given in terms of the RMSD values with respect to the R and P-state references y_R and y_P, and $\bar{y}_n$ is the offset value of the reaction coordinate chosen differently for each window. The force constant used was k = 10 kcal/mol Å^2, set up using the CONS RMSD module of CHARMM. All RMSD values with respect to the references were calculated using a common set of non-hydrogen atoms in the reference R and P-state crystal structures. Late-stage coordinates of the sampling sets reported in Woo (2007) closest to each window in the reaction coordinate space in the current simulation setup were used as initial structures. The sampling time was 5.7 ns per window on average, with all windows sampled longer than 4.7 ns. The minima of constraints, $\bar{y}_n$, were chosen to produce optimal overlaps of histograms along the one-dimensional (1D) profile of Δy: most were evenly spaced across the sampled region, but three extra windows were added to enhance the overlap.

Free energy analysis and convergence tests

The histograms from the umbrella sampling were used in the weighted histogram analysis method (WHAM) (Kumar et al. 1992; Souaille and Roux 2001). Convergence of the 1D free energy profile for the overall recovery stroke was assessed by performing WHAM using different overlapping segments of time series of 0.5 ns duration, each separated by 0.1 ns in time. The results showed consistent downward convergence trends up to ~2 ns, after which the downward drift was largely replaced by fluctuations around an average. The estimate shown in Fig. 2b was obtained by excluding the initial 2.8 ns and performing partial time series WHAM analysis over the subsets of this data to obtain the error bars. For the two-dimensional (2D) landscapes shown in Figs. 2 and 4, all available data excluding the initial 1.0 ns were used. To ensure that the qualitative features of the 2D landscapes do not depend on the sampling time, the results presented were also compared with versions obtained using the 0.5 ~ 3.0 ns segments of the time series.

1D and 2D landscapes

The procedure to generate the 1D and 2D landscapes using WHAM can be summarized as follows (Souaille and Roux 2001): the unbiased distribution $P(\Delta y, x)$ as a function of the RMSD reaction coordinate Δy and a second structural reaction coordinate x is given in terms of the biased distribution $P_i^*(\Delta y, x)$ from simulation i as

$$P(\Delta y, x) = \frac{\sum_i N_i P_i^*(\Delta y, x)}{\sum_i N_i \mathrm{e}^{-\beta[u_i(\Delta y, x) - f_i]}}, \quad (1)$$

where the free energy offset constant f_i is determined by

$$\mathrm{e}^{-\beta f_i} = \int \mathrm{d}\Delta y \int \mathrm{d}x \mathrm{e}^{-\beta u_i(\Delta y, x)} P(\Delta y, x) \quad (2)$$

In Eqs.(1–2), which are solved self-consistently by iteration, u_i is the constraining potential for the simulation

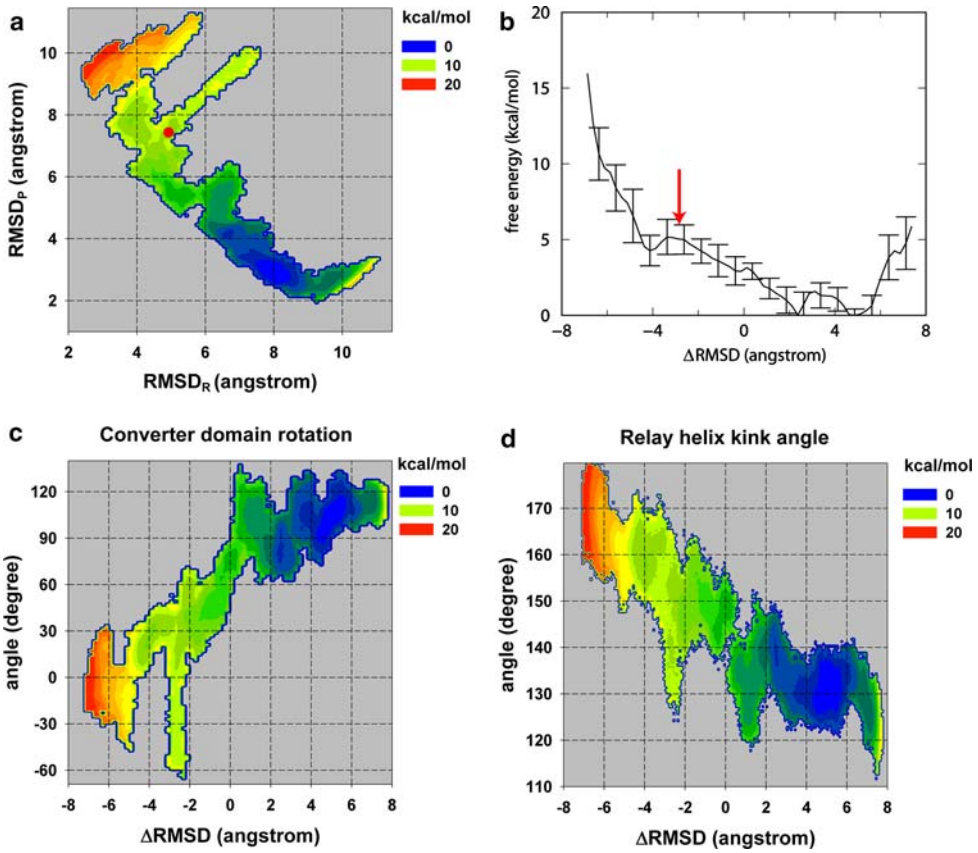

Fig. 2 Free energy landscapes of large scale conformational changes. **a** 2D landscape of recovery stroke as a function of $RMSD_R$ (y_R) and $RMSD_P$ (y_P). **b** Free energy profile as a function of the ΔRMSD (Δy) reaction coordinate. The line represents the result obtained from free energy analysis using data collected excluding initial 2.8 ns. The *error bars* represent the standard deviations of the profiles from 13 partial time series segments of 0.5 ns duration. **c** 2D landscape of converter domain rotation. **d** 2D landscape of relay helix kink formation

(or window) i, and N_i is the number of data points in time series from the simulation i. The unbiased distribution $P(x)$ can be obtained with $P(x) = \int \mathrm{d}\Delta y P(\Delta y, x)$.

If u_i is independent of x, however, Eq. (2) can be simplified into

$$\begin{aligned} \mathrm{e}^{-\beta f_i} &= \int \mathrm{d}\Delta y \mathrm{e}^{-\beta u_i(\Delta y)} P(\Delta y) \\ &= \int \mathrm{d}\Delta y \frac{\mathrm{e}^{-\beta u_i(\Delta y)} \sum_j N_j P_j^*(\Delta y)}{\sum_j N_j \mathrm{e}^{-\beta[u_j(\Delta y) - f_j]}}, \end{aligned} \tag{3}$$

where $P_i^*(\Delta y) = \int \mathrm{d}x P_i^*(\Delta y, x)$. Eq. (3) is the standard 1D version of Eqs. (1–2). The convergence of free energy analysis therefore only requires overlaps in P_i^* (Δy) when the second reaction coordinate was not explicitly constrained during the sampling, while the 2D landscape can still be obtained from Eq. (1).

Structural parameters

The rotation angles of the recovery stroke were defined as follows (Fig. 1a, b): the converter domain angle as the dihedral angle of the centers of mass of Lys342, Phe472, Phe493, and Ala787, and the relay helix kink as the angle formed by Phe472, Phe493, and Glu503. Hydrogen bond distances were defined as those between the heavy atoms involved. In cases where there are more than one hydrogen bond possible, the shortest of the heavy atom distances was taken for each frame in the trajectories. The rotameric state of Trp507 side chain was measured in terms of the dihedral angle of atoms C, CA, CB, and CG.

Results

Overall energetics of the recovery stroke

The direct output of the umbrella sampling simulations is the free energy profile as a function of the ΔRMSD, $\Delta y = y_R - y_P$, which ranges from the minimum ($\Delta y = -8.6$ Å) to the maximum ($\Delta y = 8.6$ Å), each corresponding to the reference crystal structures of the R and P-states. Figure 2b shows the best estimate of the profile from the current sampling, where a pronounced minimum is located near $\Delta y \approx 4$ Å, corresponding to the pre-stroke conformation stable for the (unhydrolyzable) ATP-bound myosin head. The overall shape of Fig. 2b is generic to the use of RMSD reaction coordinates (Banavali and Roux 2005a; Woo and Roux 2005; Arora and Brooks

2007; Yu et al. 2007a), which has clear physical interpretations as follows: the free energy profile G is related to the probability density P of the reaction coordinate via $P(\Delta y) \propto e^{-G(\Delta y)/k_B T}$. The number of states with a given value of Δy approaches 1 at the two ideal limiting states, and at physiological temperature, the probability of having atomic fluctuations quenched to maintain all atoms at crystallographic positions is always zero. The free energy profiles therefore in general diverge logarithmically at the two limiting end-points: it is unfavorable to freeze protein atoms all at given crystal coordinates. If the given reference crystal structure constitutes one typical snapshot out of an ensemble of many closely related stable states, one obtains a free energy minimum in close proximity to the reference limiting point as in Fig. 2b. The distance between the frozen reference state ($\Delta y = 8.6$ Å) and the ensemble of states represented by the free energy minimum ($\Delta y \approx 4$ Å) provides a quantitative measure of inevitable thermal fluctuations consisting of small subdomain movements and atomic motions around the crystal structure.

In contrast, only a weak local minimum exists on the near-rigor side at $\Delta y \approx -4$ Å, not much pronounced compared to the error bars. Further insights to the stability of conformations close to the R-state reference can be obtained from the 2D landscape as a function of the RMSD values with respect to the two references (Fig. 2a). It indicates that the regions with $\Delta y < -4$ Å in Fig. 2b correspond to unphysical conformations with $y_P > 9$ Å, while y_R rarely gets below ~ 3 Å. We conclude that conformational states with $\Delta y < -4$ Å are highly unstable with bound ATP. The unfavorability of the reference R-state is consistent with the fact that ATP analog-bound scallop myosins do not crystallize in the near-rigor conformation (Houdusse et al. 2000). It is therefore reasonable to assign the neighborhood of the local minimum $\Delta y \approx -4$ Å of Fig. 2b as the starting point of the recovery stroke.

This assignment of the location of recovery stroke starting point is supported further by the computationally refined structure of actin-bound chicken skeletal myosin (Liu et al. 2006) based on the cryo-EM model of Holmes et al. (2003). The model structure corresponds to the rigor state, the stable conformation of the actin-bound myosin without nucleotides. Upon binding of an ATP, the myosin head would detach from the actin, and the conformation immediately after the detachment, the initial state of the recovery stroke, is expected to be close to the rigor configuration. We calculated the two RMSD values of this rigor model with respect to the scallop myosin reference states of the current work, which yielded $y_R = 4.9$ Å, $y_P = 7.7$ Å, and $\Delta y = -2.8$ Å (indicated by the red circle and arrow in Figs. 2a, b and 3).

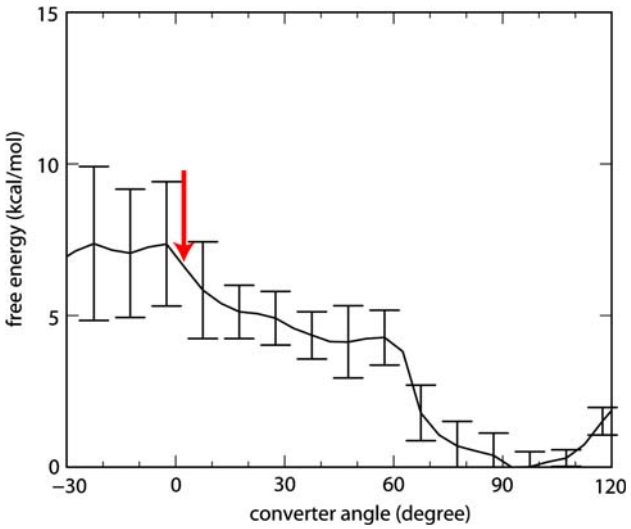

Fig. 3 1D profile as a function of the converter domain rotation angle, obtained by a reduction of the 2D landscape in Fig. 2c. The *red arrow* indicates the angle corresponding to the actin-bound rigor model

Converter domain rotation and relay helix kink

Although the sampling was performed using the ΔRMSD as the sole constraint, the resulting trajectories can be used to extract the dependence of free energy on many structural changes characteristic of the recovery stroke. In particular, 2D landscapes as functions of Δy and a second structural reaction coordinate can be obtained using WHAM (see "Methods"). Such 2D free energy landscapes reveal details of how the given structural features are coupled to the overall conformational change represented by Δy. The most prominent large scale conformational change during the recovery stroke is the swinging of the lever arm/converter domain (Geeves and Holmes 1999). We defined the converter domain rotation angle as the dihedral angle of four characteristic residues (Fig. 1a, b), with the angle of the crystallographic R-state taken as 0° and the P-state, 97.5°. The free energy change as a function of both Δy and the converter rotation angle is shown in Fig. 2c, where the transition is seen to occur roughly along the diagonal line of the plot. It indicates that the ΔRMSD reaction coordinate is closely coupled to the converter rotation angle. This close coupling supports the use of Δy as the reaction coordinate: choosing the converter rotation angle as the constrained reaction coordinate would have produced a similar landscape. Figure 3 shows the equivalent 1D profile as a function of this rotation angle, obtained by reducing the Δy dependence of the 2D landscape in Fig. 2c.

During the recovery stroke, the relay helix becomes bent, developing a kink (Fig. 1a, b) via the breaking of four backbone hydrogen bonds (His490-Glu496), a feature observed both in scallop and *Dictyostelium* myosins. The

free energy landscape with respect to the relay helix kink angle and Δy is shown in Fig. 2d, which demonstrates that the Δy reaction coordinate is also closely coupled to the relay helix kink angle. The two landscapes of Fig. 2c and d illustrate the nature of conformational changes involved in the recovery stroke as characterized by the gradual relative movements of large subdomains.

Closing of the ATP binding pocket

The hydrogen bond that forms at the active site between Gly463 of switch-2 and the γ-Pi of the bound ATP is thought to play roles in coupling the events at the active site with the larger conformational changes of myosin during the recovery stroke (Geeves and Holmes 1999). The formation of this hydrogen bond can also be used to define the open (Gly463:γ-Pi hydrogen bond broken) and closed (Gly463:γ-Pi hydrogen bond formed) states of the active site. Our sampling was performed with constraints acting only on the global Δy reaction coordinate, and more subtle structural changes, including the open/close transition, are not sampled as efficiently. Nevertheless, the 2D landscape for this hydrogen bond (Fig. 4a) suggests that in the middle of the recovery stroke ($\Delta y \approx -1$ Å, converter/lever arm angle $\approx 62°$), in addition to the stable open state, the closed state can also be locally stable. This open state with the converter "half-way up" was observed in one window where both signatures of the open/close transition, Gly463:γ-Pi (3.3 ± 0.7 Å; Fig. 4a) and Arg242:Glu465 (see below; 3.8 ± 1.9 Å; Fig. 4c) hydrogen bonds largely remained formed, which suggests the possibility that the catalytic activity could be turned on even when the converter/lever arm rotation has not been fully completed. Moving towards the end of the recovery stroke, the open state evolves into a single closed state. This trend is consistent with Yu et al.'s study (2007a) of the open/close transition within separate R-state and P-state crystal structures of *Dictyostelium* myosin. Our results shown in Fig. 4a go further and explicitly show the coupling between this open/close transition and the global conformational change.

Based on a minimum energy study, Koppole et al. (2007) have proposed that the signaling from the ATP γ-Pi to the switch-2 is in turn coupled to the relay helix via a hydrogen bond between Gly463 and Asn481 (Fig. 1c, d). We tested this hypothesis by examining the statistics of this hydrogen bond (Fig. 4b). The 2D landscape suggests that this bond remains largely formed but flexible with no appreciable coupling to the progression of the recovery stroke, which implies that its role as a coupling mechanism would be structural.

The double salt bridge that forms between Glu465 and Arg242 is a critical feature of the active site (Onishi et al. 1998; Furch et al. 1999). The formation of this salt bridge has also been used to define the active site as open or closed, with the salt bridge broken or formed, respectively (Yu et al. 2007a). The 2D landscape for the formation of the salt bridge is shown in Fig. 4c, which demonstrates that it can stay broken (open) near the initial stage of the recovery stroke at $\Delta y \approx -4$ Å, while it remains predominantly intact (closed) as the myosin approaches the P-state. This result is also consistent with the qualitative feature revealed by the statistics of the Gly463:γ-Pi hydrogen bond. It was observed that occasional excursions in sampled trajectories (typically of $\sim$0.1 ns time scale), however, do break this salt bridge, contributing to the narrow vertical "arms" in Fig. 4c.

Fluorescence probe Trp507

The residue Trp507 (501 in *Dictyostelium*) has widely been used as a fluorescence probe reflecting the open/close transition in kinetics studies of myosin (Onishi et al. 1998; Málnási-Csizmadia et al. 2001b; Kovács et al. 2002; Conibear et al. 2004; Málnási-Csizmadia et al. 2007). The probe is thought to undergo a change in its solvation environment over the course of the recovery stroke, resulting in a corresponding shift in fluorescence intensity (Geeves and Holmes 1999). This probe offers an ideal means of calibrating our sampled data with experimental studies, while providing previously unavailable, more direct molecular level interpretations of the experimental methods. We analyzed the sampled trajectories to examine the changes to the solvation environment of Trp507 during the recovery stroke using two different measures: the number of water molecules within 4.5 Å of the Trp507 side chain, and the formation of Trp507:Gln497 hydrogen bond. The latter was identified by Fischer et al. (2005) as potentially contributing to the changes in the solvation environment of Trp507. The number of water molecules solvating Trp507, shown in Fig. 4d, shows clear variations from $\sim$25 near the beginning of the recovery stroke at $\Delta y \approx -4$ Å to $\sim$10 near the midpoint at $\Delta y \approx 0$. It is then maintained at that level throughout the latter half of the large scale conformational change represented by the converter domain rotation. The statistics of the hydrogen bond between Trp507 and Gln497 shows analogous trends (Fig. 4e), where the bond formation/dissociation is reversible for $\Delta y < 0$, while for $\Delta y > 0$, the hydrogen bond remains predominantly formed. In particular, the changes to both signatures of the Trp507 fluorescence are closely matched with the open/close transition of Fig. 4a and c, while roughly coinciding with the earlier half of the global converter domain rotation (30° → 70°; Fig. 2c).

Our data allow us to go further and obtain a quantitative estimate of the free energy associated with the solvation

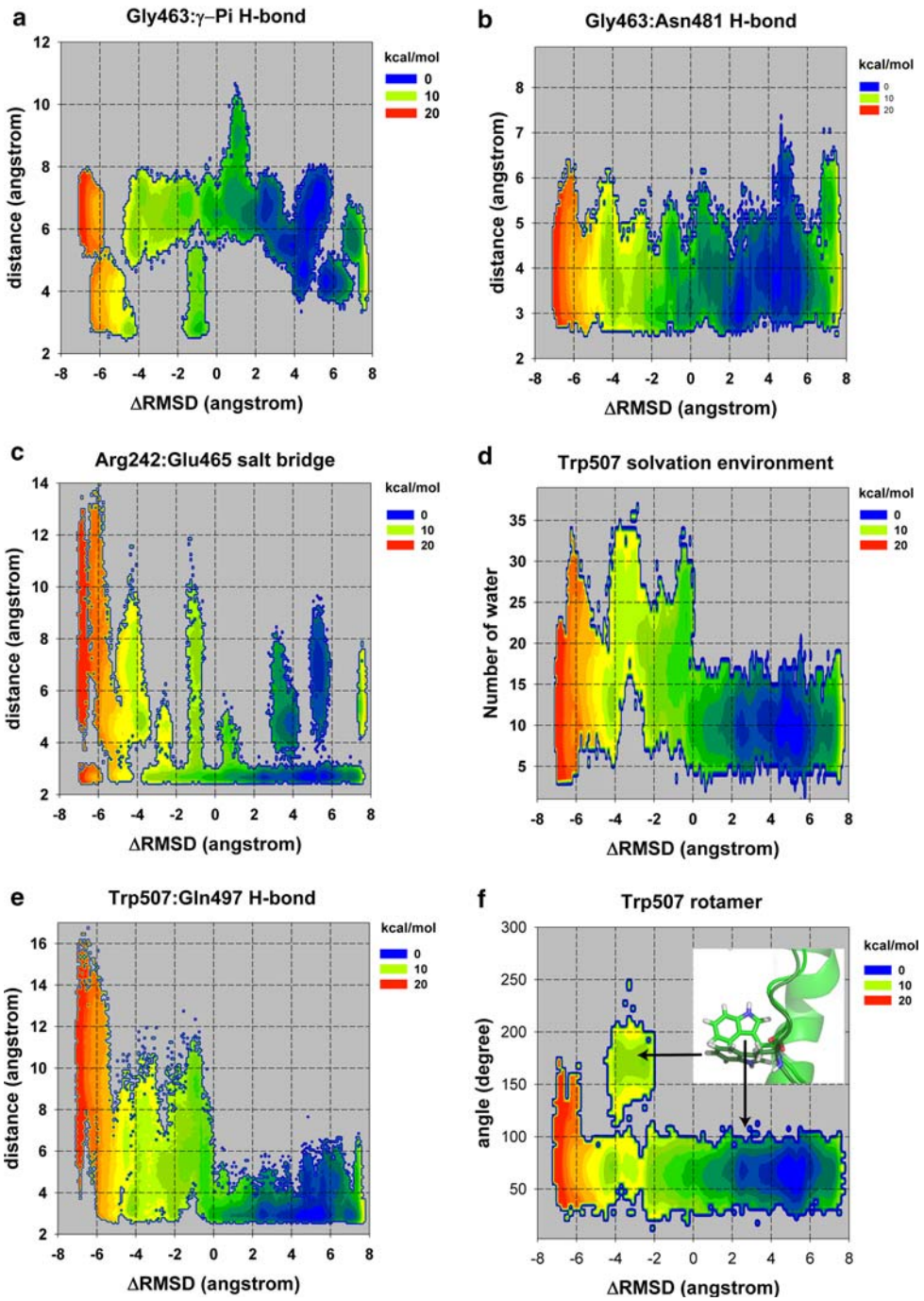

Fig. 4 2D landscapes of smaller scale conformational changes. **a** Gly463:γ-Pi hydrogen bond. **b** Gly463:Asn481 hydrogen bond. **c** Arg242:Glu465 double salt bridge. **d** solvation environment of Trp507, defined as the number of water molecules within 4.5 Å of its side chain. **e** Trp507:Gln497 hydrogen bond. **f** Trp507 rotamers, where the angle shown is the dihedral angle of its side chain rotation. The inset shows superimposed snapshots of the two rotamers observed in the R-state

environment change of Trp507. Via a reduction of the 2D landscape shown in Fig. 4e, we obtained the free energy profile as a function of the Trp507:Gln497 hydrogen bond distance representing the solvation environment change. The profile shown in Fig. 5 gives an estimate of -1.3 ± 0.3 kcal/mole for this solvation change in the direction from the open (hydrogen bond reversible; $\Delta y < 0$ in Fig. 4e) to closed state (hydrogen bond formed; $\Delta y > 0$ in Fig. 4e) accompanying the recovery stroke, in reasonable agreement with the experimental value of -0.33 kcal/mole reported for the AMP·BeF_x-bound *Dictyostelium* myosin at 23° (Málnási-Csizmadia et al. 2001b).

Fluorescence experiments utilizing Trp507 have also provided evidences for the existence of up to three distinct local environments in both open and closed states (Málnási-Csizmadia et al. 2001a), which can be associated with multiple rotameric states of its side chain, in addition to the hydrogen bond formation with Gln497. We have analyzed our collected data to probe such rotameric states, shown in Fig. 4f: two distinct and stable rotamers were observed

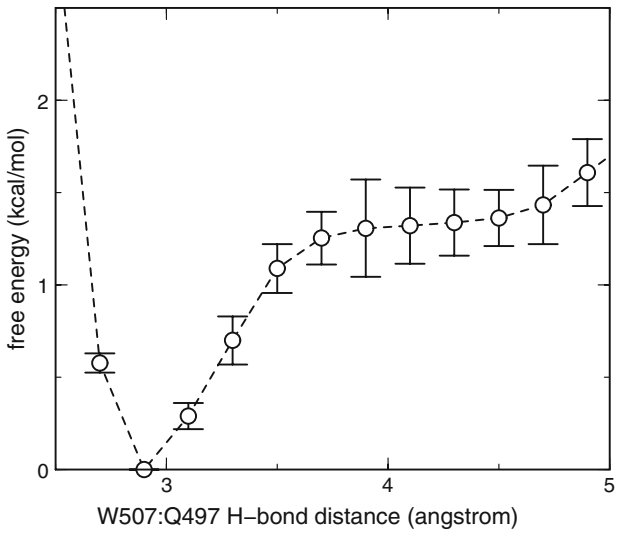

Fig. 5 1D profile of free energy as a function of the Trp507:Gln497 hydrogen bond. The solid line shows the result of free energy analysis using the whole time series excluding initial 2.8 ns. *Error bars* show the standard deviations of 7 partial time series of 0.5 ns duration

near the start of the recovery stroke at $\Delta y = -4$ Å, while within the rest of the conformational space, only one of them appears to dominate. The existence of multiple rotamers in the R-state is consistent with the disordered nature of the relay loop in many *Dictyostelium* structures and that of the Trp side chain in scallop myosins, in addition to the crystal structure of Kliche et al. (2001) for the open state myosin, in which two distinct rotamers of the Trp residue were observed within a single unit cell.

Discussion

Our results obtained from the sampling of conformational states spanning the recovery stroke support the experiments using the Trp507 fluorescence change as a probe of the open/close transition. In addition, based on the energetics of the signatures of Trp507 solvation environment changes in Fig. 4d and e in comparison with the structural changes represented in Fig. 1e and f, the following molecular level interpretation of the fluorescence shift can be made: as the recovery stroke progresses with the converter domain rotation, the SH1 helix (red in Fig. 1) next to the converter domain approaches the relay helix and Trp507 in particular, expelling roughly half of water molecules within its solvation shell. This de-solvation results in the shift of the Trp507:Gln497 hydrogen bond equilibrium from being reversible ($\Delta y < 0$) to predominantly formed ($\Delta y > 0$), since water molecules become relatively inaccessible and unable to substitute Gln497 for hydrogen bond formations with Trp507 as efficiently in the P-state as in the R-state.

Qualitative aspects of the large scale structural changes associated with the recovery stroke uncovered by our study largely agree with those anticipated in previous structural, minimum energy, and local MD studies. In addition to providing the energetics of changes inaccessible in minimum energy approaches, our results, however, also show a number of differences in details of the changes: the converter domain rotation angle of up to 90° is larger than the angle considered in the minimum energy study of Fischer et al. (2005). This difference can be understood as a result of the entropic effects not accounted for in minimum energy studies: Fig. 3 shows that the range of converter orientations with angles from 0° to 60° essentially has a flat free energy landscape. In the early stages of the recovery stroke, it is therefore likely that the converter domain orientation fluctuates widely with no particular orientation preferred. A more appreciable drop in free energy occurs only for angles larger than 60°, which also coincides with the beginning of the closing of binding pocket in Fig. 4a. The significance of entropic effects is also illustrated in the contrast between the deterministic scenario proposed by Fischer et al. (2005) involving a two-phase progression, and the gradual change of relay helix kink angle observed in Fig. 2d.

In addition, the overall qualitative features of the structural signatures associated with the open/close transition shown in Fig. 4 suggest that the open state consists of an ensemble of relatively broader range of structures compared to the closed state, and is characterized by large thermal fluctuations: Gly463-γPi hydrogen bond, Arg242-Glu465 salt bridge, and Trp507-Gln497 hydrogen bond can all be either broken or formed in the open state. Such a feature observed here is also consistent with experimental trends in *Dictyostelium* crystal structures, where the relay helix/loop is disordered in many structures of the open form.

The umbrella sampling of this work was performed using the ΔRMSD as the sole constraint, in contrast to the earlier testing of the methodology (Woo 2007) where both y_R and y_P were constrained in the 2D reaction coordinate space along the diagonal. The current full-scale sampling thus allows for spontaneous explorations of the sampling trajectories away from the intermediate conformational states along the diagonal line. The collected statistics of Fig. 2a, however, indicate that the minimum free energy path does not deviate from the diagonal line appreciably. This feature is consistent with the relative simplicity of the conformational changes involved in the recovery stroke, where the bulk of total RMSD between the two reference states consists of rigid body type rearrangements of subdomains (Houdusse et al. 2000). It is in principle possible for a sampled trajectory to deviate from the diagonal significantly, for example by increasing both y_R and y_P

together while keeping the difference constant and thereby without increasing the energetic costs associated with the constraint. An example of such an excursion was indeed observed in one window (whose trajectory however returned to the diagonal region eventually), which is responsible for the narrow "arm" protruding on the 2D landscape in Fig. 2a and c. The rarity of such deviations (one in 34 windows) nevertheless suggests that the real pathway traversed by the protein likely lies close to the diagonal line, which offers the most economical route of achieving the conformational change.

The possibility of excursions in the converter domain orientation away from the path connecting the reference R and P-states near the R-state limit can also be considered as another evidence suggesting the relative flexibility of the near-rigor conformation of detached myosin head. In particular, for scallop myosin, based on crystallographic evidences, Houdusse et al. (1999) and Himmel et al. (2002) have proposed the existence of an "internally uncoupled" state distinct from the R and P-states, where the orientation of the converter domain lies away from the R-state in the opposite direction from the normal recovery stroke, and the SH2 helix is melted such that the converter/lever arm becomes decoupled from the myosin head. The particular lever arm orientation of this "detached" state crystal structure (Houdusse et al. 1999) is roughly coplanar with the R and P-states (with converter angle $-33°$ in our definition) and $\Delta y = -4$ Å. The "excursion" in our trajectory was in a direction perpendicular to the plane of R and P-state references (in which the SH2 helix remained intact), which however reached angles up to $-60°$ (Fig. 1c). However, the converter domain in the "detached" state is decoupled from the myosin body, and the particular orientation shown in the crystal structure is likely to be only an example of a large range of possible states. Our observation therefore appears to support the existence of such decoupled states close to the R-state reference.

In the mechanical description of cause and effect, conformational changes of the myosin head can be thought of as initiated by a switching event involving substrates, which for the recovery stroke would be the binding of ATP and the dissociation from actin filament. The sensing of the presence of γ-Pi in the binding pocket via the approach of switch-2 has thus been proposed previously as the triggering event beginning the recovery stroke, relayed in turn to the converter domain, causing its rotation via the relay helix (Fischer et al. 2005). The large entropic contribution to the free energy as evidenced by the experimentally measured entropy value (Málnási-Csizmadia et al. 2001b), however, suggests that such couplings between the binding site and the rest of myosin subdomains are relatively weak when the myosin head is detached from actin. The overall mechanism of the recovery stroke preparing the myosin head for ATP hydrolysis and re-binding to actin appears rather to rely on loose, shift-in-equilibrium type of changes, where the converter domain in the 'up' orientation favors the closed state of the binding pocket (Fig. 4a and c). The motor domain is therefore likely to have the binding pocket closed when the converter/lever arm is in the 'up' position, minimizing the chances of hydrolyzing ATP with the lever arm in the "wrong" orientation (Geeves and Holmes 1999). This trend has been clearly demonstrated by a recent work by Málnási-Csizmadia et al. (2007), who showed that structural perturbations caused by mutations affecting subdomain interfaces produce shifts in the recovery stroke equilibrium and the ATPase function of myosin.

Our study has been confined to the energetics of conformational changes of a myosin head with bound ATP, detached from actin. A possibility that one might consider based on the current results, however, is that myosins could have evolved to keep the inter-domain coupling loose when detached from actin. They can thereby maintain the recovery stroke reversible by counter-balancing the enthalpy increase with an entropy increase, thus minimizing wasteful dissipation of free energy. The results indicating that the coupling of the switch-2:γ-Pi bond to converter domain rotation is weak and dominated by fluctuations (Fig. 4a), for example, support such a scenario. The binding to actin, on the other hand, presumably tightens the inter-domain coupling, effectively eliminating the entropic effect and making the power stroke predominantly downhill in enthalpy and free energy. The structural study based on cryo-EM data of actin-bound myosin (Holmes et al. 2003), where evidences for the closing of the cleft between the upper and lower 50 K domains upon actin binding have been found, supports such expectations. The biochemical study by Gyimesi et al. (2008) also provide direct experimental evidences supporting such a view, where it was shown that the reverse recovery stroke of myosin is a slow, rate-limiting step in the absence of actin. The actin activation facilitates this power stroke (rather than the Pi-release), making it practically irreversible. Although our results do not provide direct estimates of how much fraction of the overall free energy change arises from entropic origin, the landscapes of Figs. 2 and 4 clearly demonstrate that the trends in most of structural signatures of the recovery stroke and open/close transition exhibit large thermal fluctuations. It will be of interest, in this sense, to compare the current results with those that could be obtained from analogous conformational MD samplings of an actin-bound myosin.

Acknowledgments Computations were performed in part on the resources of the National Science Foundation Terascale Computing System at the Pittsburgh Supercomputing Center, National Center for Supercomputing Applications, and Indiana University Big Red. We thank Josh Baker and Joe Cline for helpful comments.

References

Arora K, Brooks CLIII (2007) Large-scale allosteric conformational transitions of adenylate kinase appear to involve a population-shift mechanism. Proc Natl Acad Sci USA 104:18496–18501. doi:10.1073/pnas.0706443104

Banavali NK, Roux B (2005a) Free energy landscape of A-DNA to B-DNA conversion in aqueous solution. J Am Chem Soc 127:6866–6876. doi:10.1021/ja050482k

Banavali NK, Roux B (2005b) The N-terminal end of the catalytic domain of Src kinase Hck is a conformational switch implicated in long-range allosteric regulation. Structure 13:1715–1723. doi:10.1016/j.str.2005.09.005

Baker JE, Brust-Mascher I, Ramachandran S, LaConte LE, Thomas DD (1998) A large and distinct rotation of the myosin light chain domain occurs upon muscle contraction. Proc Natl Acad Sci USA 95:2944–2949. doi:10.1073/pnas.95.6.2944

Bauer CB, Holden HM, Thoden JB, Smith R, Rayment I (2000) X-ray structures of the apo and MgATP-bound states of *Dictyostelium discoideum* myosin motor domain. J Biol Chem 275:38494–38499. doi:10.1074/jbc.M005585200

Brooks BR, Bruccoleri RE, Olafson BD, States DJ, Swaminathan S, Karplus M (1983) CHARMM: A program for macromolecular energy, minimization, and dynamics calculations. J Comput Chem 4:187–217. doi:10.1002/jcc.540040211

Burghardt TP, Hu JY, Ajtai K (2007) Myosin dynamics on the millisecond time scale. Biophys Chem 131:15–28. doi:10.1016/j.bpc.2007.08.008

Conibear PB, Málnási-Csizmadia A, Bagshaw CR (2004) The effect of F-actin on the relay helix position of myosin II, as revealed by tryptophan fluorescence, and its implications for mechanochemical coupling. Biochemistry 43:15404–15417. doi:10.1021/bi048338j

Darden T, York D, Pederson L (1993) Particle mesh Ewald: an *N*log *N* method for Ewald sums in large systems. J Chem Phys 98:10089–10092. doi:10.1063/1.464397

Dominguez R, Freyzon Y, Trybus KM, Cohen C (1998) Crystal structure of a verterbrate smooth muscle myosin motor domain and its complex with the essential light chain: visualization of the pre-power stroke state. Cell 94:559–571. doi:10.1016/S0092-8674(00)81598-6

Faraldo-Gómez J, Roux B (2007) On the importance of a funneled energy landscape for the assembly and regulation of multidomain Src tyrosine kinases. Proc Natl Acad Sci USA 104:13643–13648. doi:10.1073/pnas.0704041104

Fischer S, Windshügel B, Horak D, Holmes KC, Smith JC (2005) Structural mechanism of the recovery stroke in the myosin molecular motor. Proc Natl Acad Sci USA 102:6873–6878. doi:10.1073/pnas.0408784102

Fisher AJ, Smith CA, Thoden JB, Smith R, Sutoh K, Holden HM et al (1995) X-ray structures of the myosin motor domain of Dictyostelium discoideum complexed with MgADP·BeF_x and MgADP·AlF_4^-. Biochemistry 34:8960–8972. doi:10.1021/bi00028a004

Furch M, Fujita-Becker S, Geeves MA, Holmes KC, Manstein DJ (1999) Role of the salt-bridge between switch-1 and switch-2 of *Dictyostelium* myosin. J Mol Biol 290:797–809. doi:10.1006/jmbi.1999.2921

Ganoth A, Friedman R, Nachliel E, Gutman M (2006) A molecular dynamics study and free energy analysis of complexes between the Mlc1p protein and two IQ motif peptides. Biophys J 91:2436–2450. doi:10.1529/biophysj.106.085399

Ganoth A, Nachliel E, Friedman R, Gutman M (2007) Myosin V movement: Lessons from molecular dynamics studies of IQ peptides in the lever arm. Biochemistry 46:14524–14536. doi:10.1021/bi701342y

Geeves MA, Holmes KC (1999) Structural mechanism of muscle contraction. Annu Rev Biochem 68:687–728. doi:10.1146/annurev.biochem.68.1.687

Gourinath S, Himmel DM, Brown JH, Reshetnikova L, Szent-Györgyi AG, Cohen C (2003) Crystal structure of scallop myosin S1 in the pre-power stroke state to 2.6 Å resolution: Flexibility and function in the head. Structure 11:1621–1627. doi:10.1016/j.str.2003.10.013

Gulick AM, Bauer CB, Thoden JB, Rayment I (1997) X-ray structures of the MgADP, MgATPγS, MgAMMPNP complexes of the *Dictyostelium discoideum* myosin motor domain. Biochemistry 36:11619–11628. doi:10.1021/bi9712596

Gyimesi M, Kintses B, Bodor A, Perczel A, Fischer S, Bagshaw CR (2008) The mechanism of the reverse recovery step, phosphate release, and actin activation of *Dictyostelilum* myosin II. J Biol Chem 283:8153–8163. doi:10.1074/jbc.M708863200

Himmel DM, Gourinath S, Reshetnikova L, Shen Y, Szent-Györgyi AG, Cohen C (2002) Crystallographic findings on the internally uncoupled and near-rigor states of myosin: Further insights into the mechanics of the motor. Proc Natl Acad Sci USA 99:12645–12650. doi:10.1073/pnas.202476799

Holmes KC, Angert I, Kull FJ, Jahn W, Schröder RR (2003) Electron cryo-microscopy shows how strong binding of myosin to actin releases nucleotide. Nature 425:423–427. doi:10.1038/nature02005

Houdusse A, Sweeney HL (2001) Myosin motors: Missing structures and hidden springs. Curr Opin Struct Biol 11:182–194. doi:10.1016/S0959-440X(00)00188-3

Houdusse A, Kalabokis VN, Himmel D, Szent-Györgyi AG, Cohen C (1999) Atomic structure of scallop myosin subfragment S1 complexed with MgADP: A novel conformation of the myosin head. Cell 97:459–470. doi:10.1016/S0092-8674(00)80756-4

Houdusse A, Szent-Györgyi AG, Cohen C (2000) Three conformational states of scallop myosin S1. Proc Natl Acad Sci USA 97:11238–11243. doi:10.1073/pnas.200376897

Ishijima A, Kojima H, Higuchi H, Harada Y, Funatsu T, Yanagida T (1996) Multiple- and single-molecule analysis of the actomyosin motor by nanometer-piconewton manipulation with a microneedle: Unitary steps and forces. Biophys J 70:383–400

Jorgensen WL, Chandrasekhar J, Madura JD, Impey RW, Klein ML (1983) Comparison of simple potential functions for simulating liquid water. J Chem Phys 79:926–935. doi:10.1063/1.445869

Kliche W, Fujita-Becker S, Kollmar M, Manstein DJ, Jon Kull F (2001) Structure of a genetically engineered molecular motor. EMBO J 20:40–46. doi:10.1093/emboj/20.1.40

Kovács M, Málnási-Csizmadia A, Woolley RJ, Bagshaw CR (2002) Analysis of nucleotide binding to *Dictyostelium* myosin II motor domains containing a single tryptophan near the active site. J Biol Chem 277:28459–28467. doi:10.1074/jbc.M202180200

Koppole S, Smith JC, Fischer S (2006) Simulations of the myosin II motor reveal a nucleotide-state sensing element that controls the recovery stroke. J Mol Biol 361:604–616. doi:10.1016/j.jmb.2006.06.022

Koppole S, Smith JC, Fischer S (2007) The structural coupling between ATPase activation and recovery stroke in the myosin II motor. Structure 15:825–837. doi:10.1016/j.str.2007.06.008

Kumar S, Bouzida D, Swendsen RH, Kollman PA, Rosenberg JM (1992) The weighted histogram analysis method for free-energy calculations on biomolecules. I. The method. J Comput Chem 13:1011–1021. doi:10.1002/jcc.540130812

Lawson JD, Pate E, Rayment I, Yount RG (2004) Molecular dynamics analysis of structural factors influencing back door

Pi release in myosin. Biophys J 86:3794–3803. doi:10.1529/biophysj.103.037390

Li G, Cui Q (2004a) Analysis of functional motions in Brownian molecular machines with an efficient block normal mode approach: Myosin-II and Ca^{2+}-ATPase. Biophys J 86:743–763

Li G, Cui Q (2004b) Mechanochemical coupling in myosin: A theoretical analysis with molecular dynamics and combined QM/MM reaction path calculations. J Phys Chem B 108:3342–3357. doi:10.1021/jp0371783

Liu Y, Scolari M, Im W, Woo HJ (2006) Protein-protein interactions in actin-myosin binding and structural effects of R405Q mutation: A molecular dynamics study. Proteins 64:156–166. doi:10.1002/prot.20993

Lymn RW, Taylor EW (1971) Mechanism of adenosine triphosphate hydrolysis by actomyosin. Biochemistry 10:4617–4624. doi:10.1021/bi00801a004

MacKerell AD Jr, Bashford D, Bellott M Jr, Dunbrack RL, Evanseck JD, Field MJ et al (1998) Al-atom empirical potential for molecular modeling and dynamics studies of proteins. J Phys Chem B 102:3586–3616. doi:10.1021/jp973084f

Málnási-Csizmadia A, Kovács M, Woolley RJ, Botchway SW, Bagshaw CR (2001a) The dynamics of the relay loop tryptophan residue in the *Dictyostelium* myosin motor domain and the origin of spectroscopic signals. J Biol Chem 276:19483–19490. doi:10.1074/jbc.M010886200

Málnási-Csizmadia A, Pearson DS, Kovács M, Woolley RJ, Geeves MA, Bagshaw CR (2001b) Kinetic resolution of a conformational transition and the ATP hydrolysis step using relaxation methods with a *Dictyostelium* myosin II mutant containing a single tryptophan residue. Biochemistry 40:12727–12737. doi:10.1021/bi010963q

Málnási-Csizmadia A, Tóth J, Pearson DS, Hetényi C, Nyitray L, Geeves MA et al (2007) Selective perturbation of the myosin recovery stroke by point mutations at the base of the lever arm affects ATP hydrolysis and phosphate release. J Biol Chem 282:17658–17664. doi:10.1074/jbc.M701447200

Mesentean S, Koppole S, Smith JC, Fischer S (2007) The principal motions involved in the coupling mechanism of the recovery stroke of the myosin motor. J Mol Biol 367:591–602. doi:10.1016/j.jmb.2006.12.058

Onishi H, Kojima S, Katoh K, Fujiwara K, Martinez HM, Morales MF (1998) Functional transitions in myosin: Formation of a critical salt-bridge and transmission of effect to the sensitive tryptophan. Proc Natl Acad Sci USA 95:6653–6658. doi:10.1073/pnas.95.12.6653

Rayment I, Rypniewski WR, Schmidt-Bäse K, Smith R, Tomchick DR, Benning MM et al (1993) Three-dimensional structure of myosin subfragment-1: A molecular motor. Science 261:50–58. doi:10.1126/science.8316857

Simmons RA, Finer JT, Chu S, Spudich JA (1996) Quantitative measurements of force and displacement using an optical trap. Biophys J 70:1813–1822

Smith CA, Rayment I (1996) X-ray structure of the Magnesium(II)·ADP·Vanadate complex of the *Dictyostelium discoideum* myosin motor domain to 1.9 Å resolution. Biochemistry 35:5404–5417. doi:10.1021/bi952633±

Souaille M, Roux B (2001) Extension to the weighted histogram analysis method: Combining umbrella sampling with free energy calculations. Comput Phys Commun 135:40–57. doi:10.1016/S0010-4655(00)00215-0

Spudich JA (2001) The myosin swinging cross-bridge model. Nat Rev Mol Cell Biol 2:387–392. doi:10.1038/35073086

Takagi F, Kikuchi M (2007) Structural change and nucleotide dissociation of myosin motor domain: Dual Gō model simulation. Biophys J 93:3820–3827. doi:10.1529/biophysj.106.103796

Vale RD, Milligan RA (2000) The way things move: Looking under the hood of molecular motor proteins. Science 288:88–95. doi:10.1126/science.288.5463.88

van Gunsteren WF, Berendsen HJC (1977) Algorithms for macromolecular dynamics and constraint dynamics. Mol Phys 34:1311–1327. doi:10.1080/00268977700102571

Woo HJ (2007) Exploration of the conformational space of myosin recovery stroke via molecular dynamics. Biophys Chem 125:127–137. doi:10.1016/j.bpc.2006.07.001

Woo HJ, Roux B (2005) Calculation of absolute protein–ligand binding free energy from computer simulations. Proc Natl Acad Sci USA 102:6825–6830. doi:10.1073/pnas.0409005102

Yu H, Ma L, Yang Y, Cui Q (2007a) Mechanical coupling in the myosin motor domain. I. Insight from equilibrium active-site simulations. PLOS Comput Biol 3:199–213. doi:10.1371/journal.pcbi.0030199

Yu H, Ma L, Yang Y, Cui Q (2007b) Mechanical coupling in the myosin motor domain. II. Analysis of critical residues. PLOS Comput Biol 3:214–230. doi:10.1371/journal.pcbi.0030214

Zheng W, Brooks BR (2005a) Identification of dynamical correlations within the myosin motor domain by the normal mode analysis of an elastic network model. J Mol Biol 346:745–759. doi:10.1016/j.jmb.2004.12.020

Zheng W, Brooks BR (2005b) Probing the local dynamics of nucleotide-binding pocket coupled to the global dynamics: Myosin versus kinesin. Biophys J 89:167–178. doi:10.1529/biophysj.105.063305